2006-6

Vector Field Path Following for Small Unmanned Aerial Vehicles

Derek R. Nelson
Northrop Grumman Corporation, derek.nelson@ngc.com

D. Blake Barber
Brigham Young University - Provo, d.blake.barber@gmail.com

Timothy W. McLain
Brigham Young University - Provo, mclain@byu.edu

Randal W. Beard
beard@byu.edu

Original Publication Citation

Nelson, D., Barber, B., McLain, T., and Beard, R. Vector Field Path Following for Small Unmanned Aerial Vehicles, Proceedings of the American Control Conference, pp. 5788-5794, June 2006, Minneapolis, Minnesota.

Vector Field Path Following for Small Unmanned Air Vehicles

Derek R. Nelson D. Blake Barber Timothy W. McLain Randal W. Beard

***Abstract*— This paper presents a new method for unmanned aerial vehicle path following using vector fields to represent desired ground track headings to direct the vehicle onto the desired path. The key feature of this approach is that ground track heading error and lateral following error approach zero asymptotically even in the presence of constant wind disturbances. Methods for following straight-line and circular-orbit paths, as well as combinations of straight lines and arcs, are presented. Experimental results validate the effectiveness of this path following approach for small air vehicles flying in high-wind conditions.**

I. Introduction

Unmanned aerial vehicles (UAVs), large and small, have demonstrated their usefulness in military applications. Furthermore, there are numerous potential uses for UAVs in civil and commercial applications and the prospects for broad impact are strong. To extend the usefulness of UAVs beyond their current applications, the capability to plan paths and to follow them precisely is of great importance. Unlike piloted vehicles, which rely on the pilot to navigate over demanding terrain or to avoid obstructions, UAVs rely on automation to provide this functionality. As applications such as urban surveillance and rural search and rescue require UAVs to fly down city streets surrounded by buildings or near the surface of abruptly changing mountainous terrain, the ability to follow pre-planned paths with precision is essential. For missions involving cooperation among a team of UAVs, precise path tracking is often crucial to achieving the cooperation objective.

For miniature aerial vehicles,[1] such as those of primary interest in this work, wind disturbances, dynamic characteristics, and the quality of sensing and control all limit the achievable tracking precision. For MAVs wind speeds are commonly 20 to 60 percent of the desired airspeed. Effective path tracking strategies must overcome the effect of this ever present disturbance.

Several approaches have been proposed for UAV trajectory tracking. An approach for tight tracking of curved trajectories is presented in [8]. For straight-line paths, the approach approximates PD control. For curved paths, an additional anticipatory control element that improves the tracking capability is implemented. The approach accommodates the addition of an adaptive element to account for disturbances such as wind. This approach is validated with flight experiments.

In [6], Kaminer et al. describe an integrated approach for developing guidance and control algorithms for autonomous vehicle trajectory tracking. Their approach builds upon the theory of gain scheduling and produces controllers for tracking trajectories that are defined in an inertial reference frame. The approach is illustrated through simulations of a small UAV.

Implicit in the notion of trajectory tracking is that the vehicle is commanded to be in a particular location at a particular time and that this location typically varies in time, thus causing the vehicle to move in the desired fashion. With fixed-wing MAVs, the desired position is constantly moving (at the desired air speed). The approach of tracking a moving point can result in significant problems for MAVs if disturbances, such as those due to wind, are not accounted for properly. If the MAV is flying into a strong wind (relative to its commanded ground speed), the progression of the trajectory point must be slowed accordingly. Similarly, if the MAV is flying down wind, the speed of the tracking point must be increased to keep the MAV from overrunning the desired position. Given that wind disturbances vary and are often not easily predicted, trajectory tracking can be very challenging in anything other than calm conditions.

Rather than pursuing the trajectory tracking approach, this research explores path following where the objective is to be *on the path* rather than at a certain point at a particular time. With path following, the time dependence of the problem is removed. In [1], [2], performance limits for reference-tracking and path-following controllers are investigated and the difference between them is highlighted. It is shown that there is not a fundamental performance limitation for path following for systems with unstable zero dynamics as there is for reference tracking.

Building on the work presented in [5] on maneuver modified trajectory tracking, Encarnação and Pascoal develop an approach that combines the features of trajectory tracking and path following for marine vehicles [4]. Similar to this work is that of Skjetne, et al. [10] which develops an output maneuvering method composed of two tasks: forcing the output to converge to the desired path and then satisfying a desired speed assignment along the path. The method is demonstrated using a marine vessel simulation.

The work presented in this paper builds on the concept of path following through the construction of vector fields surrounding the path to be followed. The vectors of the fields provide heading commands to guide the MAV toward the desired path. As with other path following methods, the objective is not to track a moving point, but to get onto

D. Nelson is with Northrop Grumman Corporation, San Diego, CA 92127, USA derek.nelson@ngc.com

B. Barber and T. McLain are with the Department of Mechanical Engineering, Brigham Young University, Provo, UT 84602, USA d.blake.barber@gmail.com, mclain@byu.edu

R. Beard is with the Department of Electrical and Computer Engineering, Brigham Young University, Provo, UT 84602, USA beard@ee.byu.edu

[1]We consider miniature aerial vehicles to be those with wingspans in the 0.3 m to 2 m range and micro aerial vehicles to be those with wingspans under 0.3 m. Here the abbreviation MAV denotes *miniature* aerial vehicle.

the path while flying at a prescribed airspeed. A unique contribution of this paper is the utilization of ground track heading in the path following control, which in combination with the vector field strategy, guarantees that following errors asymptotically approach zero even in the presence of constant wind disturbances. Implementation of the approach is feasible on small MAVs and experimental results validate the potential value of the approach for MAVs flying in windy conditions.

II. Problem Description

To achieve accurate path following for MAVs in the presence of wind, the proposed method calculates a vector field around the path to be tracked. The vectors in the field are directed toward the path to be followed and in the desired direction of flight. The vectors in the field serve as heading commands to the MAV. The method is currently applicable to paths composed of straight lines and arcs. This restriction is insignificant for most practical applications. Figure 1 shows examples of vector fields for linear and circular paths.

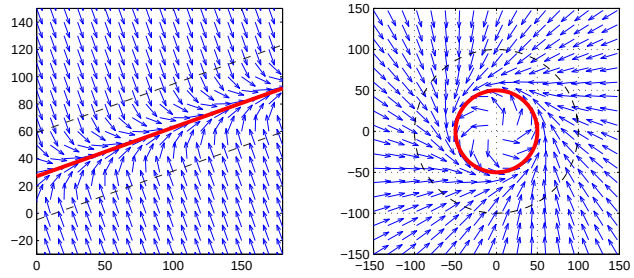

Fig. 1. Vector fields for linear and circular paths.

The notion of vector fields is similar to that of potential fields, which have been widely used as a tool for path planning in the robotics community (see e.g., [7]). It has also been suggested in [9] that potential fields can be used in UAV navigation for obstacle and collision avoidance applications. The method of [9] provides a way for groups of UAVs to use the gradient of a potential field to navigate through heavily populated areas safely while still aggressively approaching their targets. Vector fields are different from potential fields in that they do not necessarily represent the gradient of a potential. Rather, the vector field simply indicates a desired direction of travel.

This paper considers the navigation of a fixed-wing MAV with the assumption that altitude and airspeed (V) are held constant (or nearly so) by the control of the longitudinal dynamics. The following is a simple model of the navigational dynamics that will be used to study the path following behavior of the proposed approach:

$$\dot{x} = V\cos\psi + W_x \tag{1}$$
$$\dot{y} = V\sin\psi + W_y \tag{2}$$

where (W_x, W_y) represent the x and y components of the wind velocity. Heading (ψ) will be controlled by the vector field path following approaches presented in this paper. An alternative representation of these equations can be developed by noting the relationship between groundspeed (S), airspeed (V), and wind speed (W) as depicted in Figure 2:

$$\dot{x} = V_x + W_x = S_x \tag{3}$$
$$\dot{y} = V_y + W_y = S_y. \tag{4}$$

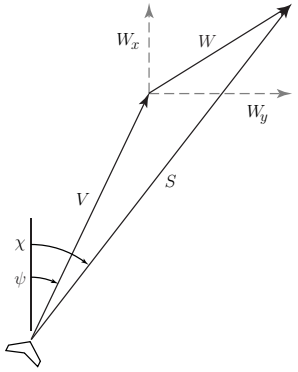

Fig. 2. Relationship between V, W, and S.

Drawing on (3) and (4) and the definition of groundtrack heading (χ) shown in Figure 2, (1) and (2) can be expressed as

$$\dot{x} = S\cos\chi \tag{5}$$
$$\dot{y} = S\sin\chi \tag{6}$$

The key distinction is that the equations of motion are expressed in terms of groundspeed and ground-track heading and are independent of the wind velocity. When ground-based measurements are used in conjunction with the vector field approach to control the path of the vehicle, wind-disturbance rejection will be improved dramatically, which is vitally important for small, low-speed MAVs. We will assume that the MAV is equipped with an autopilot that implements a ground track heading hold loop and that the resulting dynamics are represented by the first order system

$$\dot{\chi} = \alpha\left(\chi^c - \chi\right), \tag{7}$$

where χ^c is the commanded ground track heading, and α is a known positive constant.

In the development and analysis of the vector field approach that follows, two primitive path types are considered: straight lines and circular orbits. Circular arcs are treated similarly to complete orbits. The approach is easily extended to paths composed of multiple segments of arcs, orbits, and straight lines.

III. Technical Approach

A. Straight Path Following

Vector Field Construction: Consider the straight-line path illustrated in the first frame of Figure 1 by the solid line segment. In order to follow this path, a vector field of desired ground track headings is constructed. When the MAV is far away from the line (lateral distance greater than 2 to 3 times the minimum turn radius) the objective is to fly toward the path. As the MAV approaches the path, the desired heading transitions from approaching the path to flying along the

path. The transition region around the path is indicated by dashed lines which lie at a distance τ on each side of the path. Outside the transition region, the desired heading or entry angle, χ^e is constant. Once inside the transition region, the desired heading begins to transition from χ^e to the heading along the desired path, χ^f. The rate of transition is controlled by a gain, $k \geq 1$.

A complete list of the variables used for the straight line following algorithm is shown in Table I. The navigational dynamics found in (5) and (6) were used in the development of the algorithm and in the stability proof for straight line following, and an outline of the algorithm can be found in Algorithm 1. The basic idea is to find where the MAV is inside the vector field and then command a heading that will result in the MAV matching the desired heading as defined by the field. The parameters τ, χ^e, and k can be tuned, based on the capabilities of the MAV, in order to achieve the desired performance.

TABLE I

VARIABLES FOR STRAIGHT LINE FOLLOWING

Variable	Description
χ^f	heading from waypoint 1 to 2
s^*	MAV progress along path, $s^* \in [0, 1]$
ϵ	lateral tracking error
τ	transition region boundary distance
w_1, w_{1x}, w_{1y}	waypoint 1 and its north and east components
ρ	the side of the path that the MAV is on, having a value of ± 1
$z = (x, y)^T$	current location of the MAV
χ_c	commanded heading
χ^e	entry heading angle ($0 < \chi^e < \frac{\pi}{2}$)
k	transition gain, $k > 1$

Algorithm 1 Vector Field Construction Algorithm (Constant altitude).

$\chi^f \leftarrow \text{atan2}(w_{2y} - w_{1y}, w_{2x} - w_{1x})$ { Calculate heading from waypoint 1 to waypoint 2. }
$s^* \leftarrow \frac{(z-w_1)^T(w_2-w_1)}{\|w_2-w_1\|^2}$ { Calculate position of MAV along path. }
$\epsilon \leftarrow \|z - (s^*(w_2 - w_1) + w_1)\|$ { Calculate distance of MAV from path. }
$\rho \leftarrow \text{sign}\left[(w_2 - w_1) \times (z - w_1)\right]$ { Calculate which side of path MAV is on. }
if $s^* > 1$ **then** {MAV is past second waypoint}
    Switch to next waypoint
else
    $\epsilon \leftarrow \rho\epsilon$
    if $|\epsilon| > \tau$ **then** {Distance from path is greater than threshhold.}
        $\chi^d \leftarrow \chi^f - \rho\chi^e$ {Set vector field heading.}
        $\chi^c \leftarrow \chi^d$ {Set commanded heading to the autopilot.}
    else
        $\chi^d \leftarrow \chi^f - (\chi^e)(\frac{\epsilon}{\tau})^k$ {Set vector field heading.}
        $\chi^c \leftarrow \chi^d - \left(\frac{k\chi^e S}{\alpha\tau^k}\right)\epsilon^{k-1}\sin\chi$ {Set commanded heading to the autopilot.}
    end if
end if

Stability Analysis: Our objective is to show that Algorithm 1 maneuvers the MAV to follow straight-line paths with asymptotically decaying error provided it can produce enough thrust to yield a positive ground speed. It will first be shown that if the MAV is initially outside the transition region that it will enter the transition region in finite time. Once inside the transition region, it will be shown that the lateral tracking and ground track heading error will approach zero asymptotically. Lyapunov arguments will be used to justify these claims.

Theorem III.1 (Outside the Transition Region) *Consider the navigational dynamics given by* (5), (6), *and* (7) *and initial conditions outside the transition region, i.e.,* $|\epsilon| \geq \tau$. *If the heading rate command is given by*

$$\chi^c = \chi^d = \chi^f - \rho\chi^e,$$

where ρ *is defined in Algorithm 1, and* $\chi^e \in (0, \frac{\pi}{2})$, *then the MAV will enter the transition region (i.e.,* $|\epsilon| < \tau$*) in finite time.*

Proof:

Without loss of generality, consider the scenario shown in Figure 3 where the path to be followed is the x-axis with $\chi^f = 0$ implying that $\epsilon = y$. Therefore we have

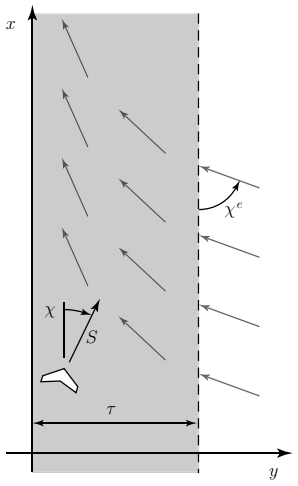

Fig. 3. Vector field geometry for $y > 0$.

that $\chi^c = \chi^d = -\rho\chi^e$. Defining $\tilde{\chi} \triangleq \chi^d - \chi$ and noting that $\rho\chi^e$ is constant gives $\dot{\tilde{\chi}} = -\alpha\tilde{\chi}$ which implies that $\tilde{\chi}(t) = e^{-\alpha t}\tilde{\chi}(t_0)$. The ground track heading will therefore converge exponentially to $-\rho\chi^e$.

Consider the case where $y(t_0) > \tau$. When $0 < \chi(t_0) < \pi$, $y(t)$ will increase initially. However, as $\chi(t)$ exponentially approaches $-\chi^e$, there exists an $\epsilon' > 0$ such that $\chi(t)$ will eventually enter the set $M \triangleq [-\pi + \epsilon', -\epsilon']$ which is easily shown to be positively invariant. When $\chi(t) \in M$, there exists an $\epsilon'' > 0$ such that $\dot{y} = S\sin\chi \leq -\epsilon''$ which implies that the decrease in y is bounded by a constant rate which implies that $y(t)$ will enter the transition region in finite time. A similar argument can be used when $y(t_0) \leq -\tau$.

□

Theorem III.2 (Inside the Transition Region) *Consider the navigational dynamics given by* (5), (6), *and* (7) *and initial conditions inside the transition region, i.e.,* $|\epsilon| < \tau$. *If the heading rate command is given by*

$$\chi^c = \chi^d - \left(\frac{k\chi^e S}{\alpha\tau^k}\right)\epsilon^{k-1}\sin\chi \tag{8}$$

where

$$\chi^d = \chi^f - (\chi^e)(\frac{\epsilon}{\tau})^k \tag{9}$$

and ϵ *is defined in Algorithm 1,* $\chi^e \in (0, \frac{\pi}{2})$, *and* $k \geq 1$, *then* $\tilde{\chi} \triangleq \chi^d - \chi \to 0$ *and* $\epsilon \to 0$ *asymptotically.*

Proof:

Again, we rotate the waypoint path to align with the x-axis and consider initial conditions where $y(t_0) > 0$, resulting in

$$\chi^d = -\chi^e\left(\frac{\rho y}{\tau}\right)^k, \tag{10}$$

Defining the Lyapunov function candidate

$$\mathcal{V}(y,\tilde{\chi}) = \frac{1}{2}y^2 + \frac{1}{2}\tilde{\chi}^2$$

and taking the derivative along the solution of the system gives

$$\begin{aligned}\dot{\mathcal{V}}(y,\tilde{\chi}) &= y\dot{y} + \tilde{\chi}\dot{\tilde{\chi}}\\ &= yS\sin\chi + \tilde{\chi}\left(\dot{\chi^d} - \dot{\chi}\right)\\ &= yS\sin(-\chi^e\left(\frac{y}{\tau}\right)^k - \tilde{\chi}) \qquad (11)\\ &\quad + \tilde{\chi}\left[\left(\frac{-k\chi^e S}{\tau^k}\right)y^{k-1}\sin\chi - \alpha\left(\chi^c - \chi\right)\right]. \qquad (12)\end{aligned}$$

Choosing χ^c as in (8) gives

$$\dot{\mathcal{V}}(y,\tilde{\chi}) = yS\sin\left(-\chi^e\left(\frac{y}{\tau}\right)^k - \tilde{\chi}\right) - \alpha\tilde{\chi}^2. \tag{13}$$

which will be negative when

$$-\pi < -\chi^e\left(\frac{y}{\tau}\right) - \tilde{\chi} < 0.$$

Using Equation (9) we see that $\dot{\mathcal{V}}$ is therefore negative semi-definite when

$$-\pi \leq \chi \leq 0,$$

and negative definite when the inequalities are replaced with strict inequalities. Define the set

$$M \triangleq \{(y,\chi) : -\pi \leq \chi \leq 0', -\tau \leq y \leq \tau\},$$

and note that M is compact and that the boundary of M is a non-invariant level curve of $\mathcal{V}$. Therefore standard Lyapunov arguments imply that M is a positively invariant set. The proof is therefore complete if we can show that the system trajectory enters M in finite time.

Differentiating $\tilde{\chi} = \chi^d - \chi$ and using Equation (8) we get that $\dot{\tilde{\chi}} = -\alpha\tilde{\chi}$, which implies that $\tilde{\chi}(t) = e^{-\alpha t}\tilde{\chi}(t_0)$. Solving for $\chi(t)$ we get

$$\chi(t) = (1 - e^{-\alpha t})\left[-\chi^e\left(\frac{y}{\tau}\right)^k\right] + e^{-\alpha t}\chi(t_0),$$

which implies that if $y(t)$ remains in the transition region then the trajectory of the system enters M in finite time. However, the initial orientation of the MAV may force the system to leave the transition region. If this happens, then from the proof of Theorem III.1 we see that the system will re-enter the transition region in finite time and that the ground track heading upon re-entry will be in the set $(-\pi, 0)$ which implies that upon re-entry, the system trajectory will be in M.

□

B. Orbit Following

Vector Field Description: The algorithm for circular orbits creates vector fields in a manner similar to the straight-line algorithm. Consider the desired orbit path shown in Figure 4. In this discussion, a counter-clockwise orbit will be considered. The development for clockwise orbits is similar with the exception of several sign changes. The desired orbit is assumed to have a known center with coordinates c_x, c_y and a known radius r. When the distance between the MAV and the center of the orbit, d, is greater than $2r$, it is desirable for the MAV to fly along a heading tangent to the orbit to be followed so that transitioning into the orbit can happen with minimal transient behavior. The desired heading for $d > 2r$ is

$$\chi^d = \gamma - \pi + \sin^{-1}\left(\frac{r}{d}\right) \tag{14}$$

where γ is defined as the heading from the center of the orbit to the MAV as shown in Figure 4.

Once inside of $2r$, the desired heading field transitions as d decreases from $2r$ to r. At $d = 2r$, the desired heading is $\chi^d = \gamma - \pi + \sin^{-1}\left(\frac{r}{d}\right) = \gamma - \frac{5\pi}{6}$. At $d = r$, $\chi^d = \gamma - \frac{\pi}{2}$. The desired heading for a counter-clockwise orbit when $d \leq 2r$ is determined by

$$\chi^d = \gamma - \frac{\pi}{2} - \frac{\pi}{3}\left(\frac{d-r}{r}\right)^k \tag{15}$$

where $k \geq 1$ is a gain determining the rate of transition. The same equation holds for $d < r$.

Since orbits are being followed, it is convenient to change the navigational dynamics to polar coordinates in terms of d and γ where the center of the orbit is the origin. From Figure 4, $x = c_x + d\cos\gamma$ and $y = c_y + d\sin\gamma$. Taking the derivative and substituting into (5) and (6) gives

$$\dot{d} = S\cos(\chi - \gamma) \tag{16}$$

$$\dot{\gamma} = \frac{S}{d}\sin(\chi - \gamma) \tag{17}$$

where the S and χ are the ground track speed and heading, respectively. As in the previous section, the dynamics for ground track heading are assumed to be given by

$$\dot{\chi} = \alpha(\chi^c - \chi). \tag{18}$$

A table listing the variables used and a summary of the orbit vector field construction algorithm can be found in Table II and Algorithm 2.

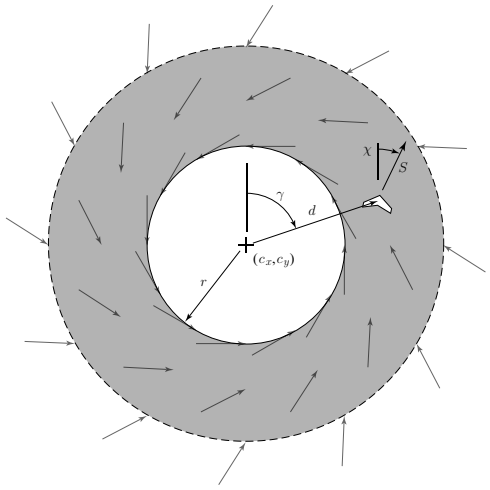

Fig. 4. Vector field geometry for orbit tracking.

TABLE II
VARIABLES FOR ORBIT FOLLOWING

Variable	Description
r	orbit radius
$z = (x, y)^T$	GPS coordinates for the MAV
$c = (c_x, c_y)^T$	GPS coordinates for the center of the orbit
k	convergence gain, $k \geq 1$
d	distance from the center of orbit to the MAV
χ^d	desired ground track heading
χ^c	commanded ground track heading

Algorithm 2 Orbit Following Vector Field Algorithm (Counter-Clockwise Direction)

Obtain current position z
$d \leftarrow \|z - c\|$ { Calculate distance to center of orbit }
if $d > 2r$ **then**
  $\chi^d \leftarrow \gamma - \pi + \sin^{-1}\left(\frac{r}{d}\right)$
  $\chi^c \leftarrow \gamma - \pi + \sin^{-1}\left(\frac{r}{d}\right) + \frac{S}{\alpha d}\sin(\chi - \gamma)$
else
  $\chi^d \leftarrow \gamma - \frac{\pi}{2} - \frac{\pi}{3}\left(\frac{d-r}{r}\right)^k$
  $\chi^c \leftarrow \chi^d - \frac{S}{\alpha d}\sin(\chi - \gamma) - \frac{kS\pi}{3r^k\alpha}\tilde{d}^{k-1}\cos(\chi - \gamma)$.
end if

Stability Analysis: Our objective is to show that Algorithm 2 maneuvers the MAV to track the prescribed orbit with with asymptotically decaying error. Again we will show that the MAV enters the transition region in finite time, and that once in transition region the tracking error goes to zero asymptotically.

Theorem III.3 (Outside of Two Radii) *Consider the navigational dynamics given by* (16), (17), *and* (18) *and an initial position that is greater than two radii from the center of the orbit. If the heading rate command is given by*

$$\chi^c = \chi^d + \frac{S}{\alpha d}\sin(\chi - \gamma) \tag{19}$$

where

$$\chi^d = \gamma - \pi + \sin^{-1}\left(\frac{r}{d}\right) \tag{20}$$

then the system enters the set $\{d \leq 2r\}$ *in finite time.*

Proof:
Define

$$\tilde{\chi} \triangleq \chi^d - \chi = \gamma - \pi + \sin^{-1}\left(\frac{r}{d}\right) - \chi.$$

Differentiating and using Equation (19) we get

$$\begin{aligned}\dot{\tilde{\chi}} &= \dot{\gamma} - \dot{\chi} \\ &= \frac{S}{d}\sin(\chi - \gamma) - \alpha(\chi^c - \chi) \\ &= \alpha\left[-\chi^c - \tilde{\chi} + \gamma - \pi + \sin^{-1}\left(\frac{r}{d}\right) + \frac{S}{\alpha d}\sin(\chi - \gamma)\right] \\ &= -\alpha\tilde{\chi},\end{aligned}$$

which implies that $\tilde{\chi}(t)$ approaches zero exponentially.

Next define $\tilde{d} \triangleq d - 2r$ and differentiate to obtain

$$\begin{aligned}\dot{\tilde{d}} &= S\cos(\chi - \gamma) = S\cos\left(\tilde{\chi} + \gamma - \pi + \sin^{-1}\left(\frac{r}{d}\right) - \gamma\right) \\ &= -S\cos\left(\tilde{\chi} - \sin^{-1}\left(\frac{r}{d}\right)\right).\end{aligned}$$

As $\tilde{\chi} \to 0$, $\dot{\tilde{d}} \to \frac{-S\sqrt{d^2 - r^2}}{r} < 0$ which implies that $\tilde{d} \to 0$ in finite time.

□

Theorem III.4 (Inside of Two Radii) *Consider the navigational dynamics given by* (16), (17), *and* (18) *and an initial position that is less than or equal to two radii from the center of the orbit. If the heading rate command is given by*

$$\chi^c = \chi^d - \frac{S}{\alpha d}\sin(\chi - \gamma) - \frac{kS\pi}{3r^k\alpha}\tilde{d}^{k-1}\cos(\chi - \gamma), \tag{21}$$

where

$$\chi^d = \gamma - \frac{\pi}{2} - \frac{\pi}{3}\left(\frac{d - r}{r}\right)^k \tag{22}$$

and $k \geq 1$, *then* $\chi \to \chi^d$ *and* $d \to r$ *asymptotically.*

Proof: Define $\tilde{d} = d - r$ and $\tilde{\chi} = \chi^d - \chi$ and consider the Lyapunov function candidate $\mathcal{V} = \frac{1}{2}\tilde{d}^2 + \frac{1}{2}\tilde{\chi}^2$. Differentiating along the trajectory of the system we obtain

$$\begin{aligned}\dot{\mathcal{V}} &= \tilde{d}S\cos(\chi - \gamma) - \alpha\tilde{\chi}^2 \\ &= \tilde{d}S\cos\left[-\frac{\pi}{2} - \frac{\pi}{3}\left(\frac{\tilde{d}}{r}\right)^k - \tilde{\chi}\right] - \alpha\tilde{\chi}^2 \\ &= \tilde{d}S\sin\left[-\frac{\pi}{3}\left(\frac{\tilde{d}}{r}\right)^k - \tilde{\chi}\right] - \alpha\tilde{\chi}^2,\end{aligned}$$

which will be negative when

$$-\pi < -\frac{\pi}{3}\left(\frac{\tilde{d}}{r}\right)^k - \tilde{\chi} < 0.$$

Using Equation (22) we see that $\dot{\mathcal{V}}$ is therefore negative semi-definite when

$$\gamma - \frac{3\pi}{2} \leq \chi \leq \gamma - \frac{\pi}{2}, \tag{23}$$

Fig. 5. (a) Kestrel autopilot. (b) Zagi airframes. (c) Ground station components.

and negative definite when the inequalities are replaced with strict inequalities. Define the compact set

$$M \triangleq \left\{ (\tilde{d}, \chi) : \gamma - \frac{3\pi}{2} \leq \chi \leq \gamma - \frac{\pi}{2}, \tilde{d} \leq 2r \right\},$$

and note that the boundary of M is a non-invariant level curve of $\mathcal{V}$. Therefore standard Lyapunov arguments imply that M is a positively invariant set. It remains to show that trajectories of the system enter M in finite time.

Differentiating $\tilde{\chi} = \chi^d - \chi$ and using Equation (21) we get that $\dot{\tilde{\chi}} = -\alpha\tilde{\chi}$, which implies that $\tilde{\chi}(t) = e^{-\alpha t}\tilde{\chi}(t_0)$. If the trajectory of the system remains inside two radii, then the exponential decay of $\tilde{\chi}$ guarantees that the system enters M in finite time. If the initial conditions are such that d initially increases beyond $2r$, then Theorem III.3 guarantees that the system will re-enter the set $\{d \leq 2r\}$ in finite time, at which point the heading will satisfy Equation (23) which implies that upon re-entry, the system trajectory will be in M.

□

IV. Results and Discussion

A. Hardware Testbed

BYU has developed a reliable and robust platform for testing unmanned air vehicles [3]. Figure 5 shows the key elements of the testbed. The first frame shows BYU's Kestrel autopilot which is equipped with a Rabbit 3400 29 MHz processor, rate gyros, accelerometers, absolute and differential pressure sensors. The autopilot measures $3.8 \times 5.1 \times 1.9$ cm and weighs 17 grams.

The second frame in Figure 5 shows the airframes used for the flight tests reported in this paper. The airframe is a 1.2 m wingspan Zagi XS EPP foam flying wing, which was selected for its durability, ease of component installation, and flight characteristics. Embedded in the airframe are the Kestrel autopilot, batteries, a 1000 mW, 900 MHz radio modem, a GPS receiver, a video transmitter, and a small analog camera.

The third frame in Figure 5 shows the ground station components. A laptop runs the Virtual Cockpit software that interfaces through a communication box to the MAVs. An RC transmitter is used as a stand-by fail-safe mechanism to facilitate safe operations.

B. Experimental Demonstration

In order to illustrate the orbit following abilities of the algorithm, the MAV was commanded to fly a series of concentric orbits with varying radii. The results are shown in Figure 6. There was wind from the south of 2 to 3 m/s which corresponds to approximately 15 to 25 percent of the commanded MAV airspeed. The maximum deviation from the desired path was about 9 m and the average lateral error was approximately 3.4 m.

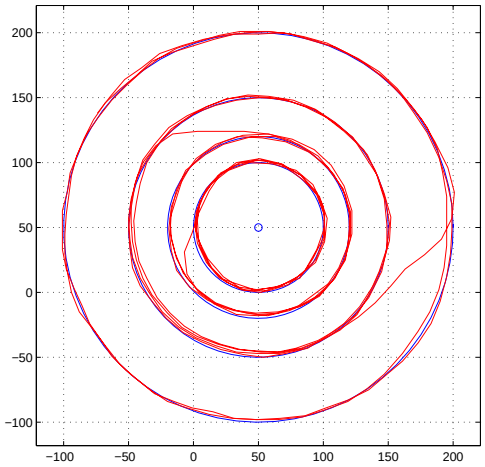

Fig. 6. Flight telemetry for orbits of 150, 100, 70, and 50 m radius.

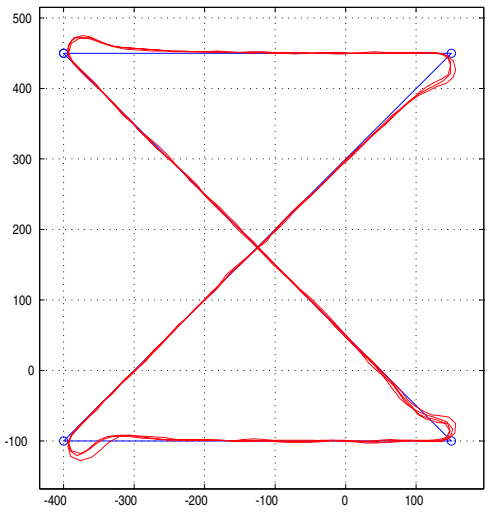

Fig. 7. Telemetry plot for straight line following.

Figure 7 illustrates the ability of the MAV to follow straight line segments with acute angles. Excluding the transient errors from the turns, the mean following error was

0.8 m with a standard deviation of 1.1 m. The wind for this flight was out of the west and was again about 2 to 3 m/s.

With the straight line and orbit following algorithms working well, a combination of the two methods was implemented and tested, with the results shown in Figure 8. Turn segments were planned to ensure that the flight path matched the length of the original straight-line paths, and utilized the orbit following algorithms to fly the arcs of the turns. Winds were 30 to 50 percent of the MAV's airspeed. The maximum deviation from the path was about 19 m and the mean distance from path and standard deviation were 3.4 m and 5.0 m respectively. Although the transitions from the straight line to the orbit portions show some lateral following errors, the actual path length flown and the desired length are very close. For the five and a half loops of the path shown in Figure 8, the desired length of the path was 14606 m. The actual distance flown was 17.5 m less than the desired distance, which is an error of only 0.12 percent.

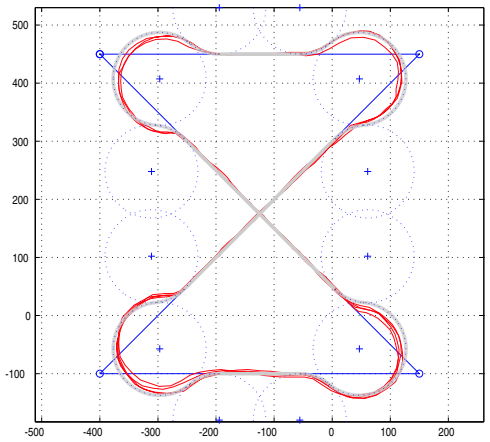

Fig. 8. Telemetry plot for equal path length following.

As a demonstration of path following in a demanding environment, Figure 9 shows a path planned through an urban type terrain along with flight data showing the path flown. Note that although these are actual flight results, the terrain is synthetic. The straight line follower was used to follow this path. The wind speed was 20 to 30 percent of the airspeed for this flight.

V. Conclusion

In this paper, a new method for MAV path following has been introduced. The idea of vector fields has been extended to constant altitude path following. It has been shown using Lyapunov stability criteria that controlling heading rate based on ground track heading and speed in a vector field yields asymptotic following for straight line and circular paths.

The effectiveness of the described following methods have been illustrated using a Zagi fixed-wing MAV and the Kestrel autopilot system. The MAV followed the desired paths with asymptotically decaying error. Minimal error was observed once the MAV had converged to the path. Vector field path following also proved effective in following smoothed paths composed of circular and straight line segments. All of the flight tests were performed in moderate wind conditions (20 to 50 percent of MAV airspeed).

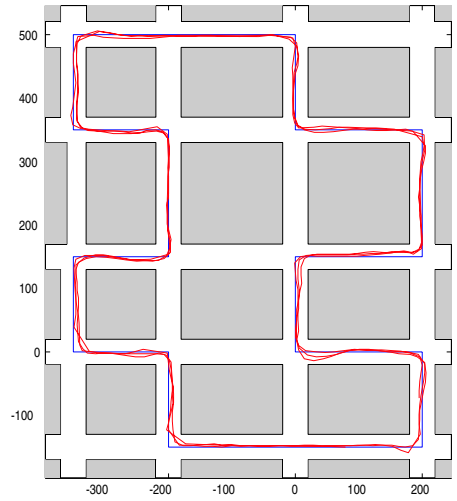

Fig. 9. Urban terrain following using straight line following.

The implementation of vector field following is straightforward and the result is a robust method for accurate path following. Controlling heading rate based on ground track heading and ground speed automatically accounts for wind conditions, providing tight following even in the presence of wind.

Acknowledgments

This work was funded by AFOSR award numbers FA9550-04-1-0209 and FA9550-04-C-0032 and by AFRL/MNK award number F08630-03-1-0017.

References

[1] P. Aguiar, D. Dačić, J. Hespanha, and P. Kokotović. Path-following or reference-tracking? An answer relaxing the limits to performance. In *Proceedings of IAV2004, 5th IFAC/EURON Symposium on Intelligent Autonomous Vehicles*, Lisbon, Portugal, 2004.

[2] P. Aguiar, J. Hespanha, and P. Kokotović. Path-following for non-minimum phase systems removes performance limitations. *IEEE Transactions on Automatic Control*, 50(2):234–239, 2005.

[3] R. Beard, D. Kingston, M. Quigley, D. Snyder, R. Christiansen, W. Johnson, T. McLain, and M. Goodrich. Autonomous vehicle technologies for small fixed wing UAVs. *AIAA Journal of Aerospace, Computing, Information, and Communication*, 2(1):92–108, January 2005.

[4] P. Encarnação and A. Pascoal. Combined trajectory tracking and path following: An application to the coordinated control of marine craft. In *Proceedings of the IEEE Conference on Decision and Control*, pages 964–969, Orlando, FL, 2001.

[5] J. Hauser and R. Hindman. Maneuver regulation from trajectory tracking: Feedback linearizable systems. In *Proceedings of the IFAC Symposium on Nonlinear Control Systems Design*, pages 595–600, Tahoe City, CA, June 1995.

[6] I. Kaminer, A. Pascoal, E. Hallberg, and C. Silvestre. Trajectory tracking for autonomous vehicles: An integrated approach to guidance and control. *AIAA Journal of Guidance, Control and Dynamics*, 21(1):29–38, 1998.

[7] O. Khatib. Real-time obstacle avoidance for manipulators and mobile robots. In *Proceedings of the IEEE International Conference on Robotics and Automation*, volume 2, pages 500–505, 1985.

[8] S. Park, J. Deyst, and J. How. A new nonlinear guidance logic for trajectory tracking. In *Proceedings of the AIAA Guidance, Navigation and Control Conference*, August 2004. AIAA-2004-4900.

[9] K. Sigurd and J. P. How. UAV trajectory design using total field collision avoidance. In *Proceedings of the AIAA Guidance, Navigation and Control Conference*, August 2003.

[10] R. Skjetne, T. Fossen, and P. Kokotović. Robust output maneuvering for a class of nonlinear systems. *Automatica*, 40:373–383, 2004.